Short Communication

Properties of TiO$_2$ Film Prepared by Anodization as Electron Transport Layer for Perovskite Solar Cells

Jia Wu, Qiyu Huang[*]

Department of Micro/Nano-Electronics, Shanghai Jiao Tong University, Shanghai 200240, China
[*]E-mail: qiyu@sjtu.edu.cn

The photovoltaic performance of perovskite solar cells (PSCs) largely depends on the characteristics of the electron transport layer (ETL). However, conventional solution-based processes may lead to obvious voids or cavities on the film. In this publication, an anodization process was proposed to transform a layer of Ti sputtered on a fluorine-doped indium tin oxide (FTO) substrate to TiO$_2$ nanotubes as an ETL for PSCs. Through a one-step anodization process in an electrolyte of ethylene glycol with NH$_4$F and H$_2$O, an integrated 500-nm-thick layer composed of a TiO$_2$ nanotube layer (mesoporous layer) and a TiO$_2$ compact layer was obtained. This method was simple and more efficient than the spin-coating process, and there were no traps between nanotube layer and compact layer. PSCs based on this ETL achieved the highest efficiency of 12.82%, which was comparable to devices whose ETLs were fabricated by a conventional spin-coating process.

1. INTRODUCTION

With the increasing demand for energy, the development of solar cells has gained increasing interest. The power conversion efficiency (PCE) of perovskite solar cells (PSCs) has made great leaps in the past ten years (from 4% in 2009 [1] to 10% in 2012 [2] and subsequently to 25.8% now [3]). It is promising to surpass silicon-based solar cells (26% [4]) and has become a research hotspot in recent years. The conventional PSC consists of a transparent anode, an electron transport layer (ETL), a perovskite absorber, a hole transport layer (HTL) and a counter electrode. As a critical part of PSCs, ETLs extract and transport electrons while blocking the diffusion of holes and play an important role in inhibiting charge recombination. The materials for ETLs can be organic materials and inorganic materials. Organic ETL materials (such as C$_{60}$[5], graphene [6], graphdiyne [7], and PCBM [8]) are usually simple to prepare but have high cost and low stability. Inorganic ETL materials (such as TiO$_2$[9],

ZnO [10], and SnO$_2$[11]) usually imply low cost, high stability and excellent electronic performance, which are more commonly adopted in PSCs. Among these alternative ETL materials, due to its wide energy gap, high electron mobility and good stability [12], TiO$_2$, which was originally used for dye-sensitized solar cells (DSSCs), has become the most widely studied material.

Several routines can be used to deposit ETLs on conductive substrates of PSCs, including solution-based processes (spin-coating [13], screen printing [14], slot-die coating [15]), atomic layer deposition (ALD) [16, 17, 18], chemical bath deposition (CBD) [19, 20], combustion [21] and electrodeposition (ED) [22]. However, these methods have certain shortcomings. For example, solution-based processes are prone to introduce defects or cavities, ALD is expensive and requires special gases, and ED easily causes harmful waste. Furthermore, they all require separate preparation of the ETL dense layer and porous layer.

To prepare a high-quality TiO$_2$ dense layer and porous layer in one simple step, an anodization method is proposed to oxidize Ti film sputtered on a fluorine-doped indium tin oxide (FTO) substrate to simultaneously create a TiO$_2$ compact layer and a TiO$_2$ nanotube layer as the ETL to synthesize a high-efficiency PSC. As such, a TiO$_2$ mesoporous (nanotube) layer and a TiO$_2$ blocking (compact) layer can be obtained by a one-step anodizing process while maintaining low trap densities and low costs. Research on the preparation of TiO$_2$ nanotubes by anodic oxidation has been fruitful. Zwilling et al. [23] first reported the anodization of Ti in a chromic acid electrolyte containing HF to synthesize an organized 500-nm-thick nanotube layer in 1999. Sergiu et al. [24] used organic electrolytes such as ethylene glycol to fabricate an almost ideal hexagonal arrangement of 250-μm-thick nanotube layers. Furthermore, there have been several reports of using anodized TiO$_2$ nanotubes as ETLs. Lei et al. [25] transferred 20.8-μm-long anodized TiO$_2$ nanotubes onto an FTO substrate and obtained a PCE of 8.07% on a DSSC based on the film. Wang et al. [26] used an anodized Ti/TiO$_2$ nanotube layer as a substrate to fabricate a solid-state flexible solar cell with an efficiency of 8.31%, where the TiO$_2$ nanotube layer was 300 nm thick.

In this article, an anodization method was adopted to synthesize TiO$_2$ nanotubes as ETLs for PSCs. TiO$_2$ nanotubes with a length of 500 nm were prepared by anodizing a Ti/FTO substrate in glycol electrolyte with NH$_4$F and H$_2$O. The film of TiO$_2$ nanotubes and the film obtained by the conventional spin-coating process were compared in several aspects, including crystal morphology, crystal size and crystallinity. PSCs with an anodized ETL achieved a maximum PCE of 12.8%. Although the result was less than the PCE of conventional PSCs with the spin-coating process, which reached 13.1%, the former showed a higher short circuit current density (31.54 mA/cm^2). The results of this research indicate that a TiO$_2$ porous layer and a compact layer can be simultaneously obtained through the anodizing process and act as an ETL for PSCs with simple steps and low costs. It is a promising method to prepare ETL for PSCs.

2. EXPERIMENTAL

To verify the feasibility of ETLs made by Ti anodization and the performance of final PSCs, two groups of PSCs using different methods were fabricated: Group A and Group B. The only difference

between these two groups was the preparation method of ETLs: anodization of Ti/FTO and conventional spin-coating were used to synthetize ETLs of Group A and Group B, respectively. The TiO_2 films and PSC devices were subsequently characterized and compared from several different aspects.

2.1 Fabrications of ETLs

One-step anodization of Ti film was used to prepare ETLs of Group A. Initially, a Ti film of ~240 nm was deposited on FTO glass (Zhuhai Kaivo, 10 ohm/sq) by magnetron sputtering (MSP-300BI, Beijing Chuangshiweina). The electrolyte was prepared by mixing 98 mL of ethylene glycol (Sinopharm Chem), 2.2 mL of DI water, and 0.335 g of NH_4F (Aladdin). Ti/FTO glass was used as the anode and placed in a homemade anodizing tank with electrolyte inside. A graphite electrode was also positioned in the tant opposite to the anode and acted as the cathode. The distance between the two electrodes was maintained at 5 cm, and the DC voltage was set to 60 V. The entire reaction proceeded at a constant temperature of 20 °C. When the anodization current dropped to the lowest point, Ti was completely anodized into TiO_2 nanotubes [27]. FTO glass was removed when the current reached the lowest point. After complete rinsing in DI water, the sample was annealed at 500 °C for 3 hours to obtain the TiO_2 ETL.

For Group B, the spin-coating method was used to synthetize the TiO_2 compact layer and mesoporous layer separately as ETLs of PSCs. The steps were explicitly elaborated in Ostapchenko et al. [28]. 0.25 M solution of 97% titanium (IV) isopropoxide (TiIP) (Acros Organics) in n-butanol (Shanghai Lingfeng) was spin-coated twice on FTO glass as a compact layer, and homemade mesoporous TiO_2 paste [29] was spin-coated twice on a compact layer as a mesoporous layer sequentially. The sample was subsequently annealed at 500 °C for 30 minutes to obtain the anatase phase.

2.2 Device fabrication

After synthetizing different ETLs by anodization and spin-coating, PSCs were assembled to verify the functionality of the anodized TiO_2 ETL. The following steps were exactly identical for Group A and Group B. To obtain higher performance, the following optimization was made to the base formula of Ostapchenko et al. [28]: ethyl cellulose was reduced to half in both Al_2O_3 and NiO pastes; 5 ml ethanol was added to the counter electrode (CE) paste; Al_2O_3 paste was spin-coated twice instead of once; the spin-coating speed of PbI solution was adjusted to 3000 rpm. PSCs with a structure of FTO/compound TiO_2 layer/mesoporous Al_2O_3/mesoporous NiO/carbon counter electrode were prepared, and the perovskite was infiltrated into the mesoporous layers following the procedure set by Ostapchenko et al. [28]. The compound TiO_2 layer in PSCs was anodized TiO_2 nanotubes for Group A and spin-coated compact TiO_2/porous TiO_2 for Group B.

2.3 Characterization

A ZEISS-Ultra field emission scanning electron microscope (FESEM) was used to observe the sample surface and cross-sectional morphologies under different magnifications. X-ray diffraction (XRD) analysis (D/max_2500pc, Rigaku) was used to analyze the crystallinity of the TiO_2 film. The TiO_2 paste for the spin-coating sample was spin-coated three times and subsequently annealed at 500 ℃ for 150 min when performing XRD analysis, since the spin-coating TiO_2 films for PSCs were too thin to reveal the crystalline structure in XRD.

I-V tests were performed under one sun-calibrated solar simulator (CHF-XM-500 W, Beijing Trusttech) with an AM 1.5G spectra filter. The active area of the samples was 0.09 cm2. A CHI-660D (CH Instruments) electrochemical workstation was used to perform the photovoltaic measurements.

3. RESULTS AND DISCUSSION

3.1 Morphology of prepared samples
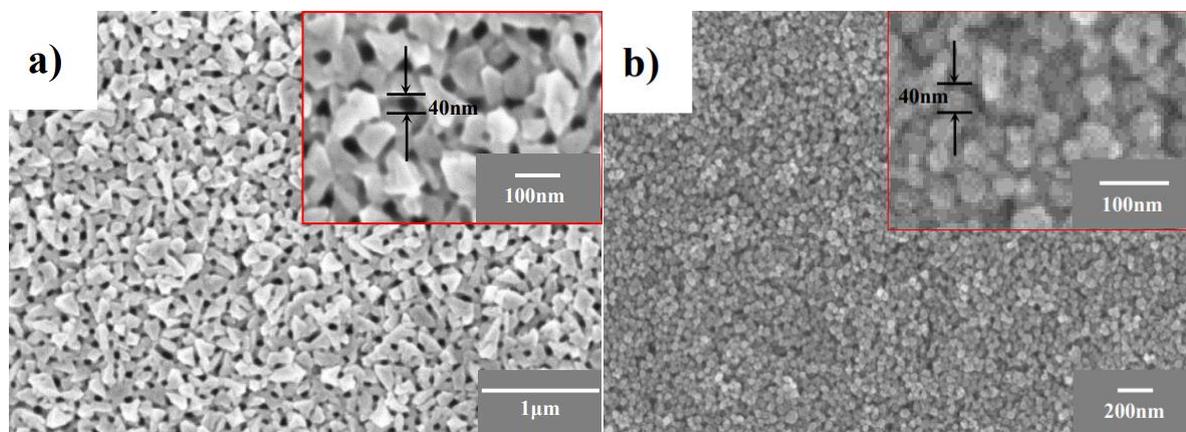
Figure 1. Top view of TiO_2 layers in each group, prepared by a) anodizing Ti/FTO substrate and annealing (Group A); b) spin-coating compact and porous TiO_2 films and annealing (Group B). The insets are close-up images of the corresponding group.

Fig. 1 shows the top-view SEM images of ETLs prepared by two different techniques, and crystalline TiO2 particles were marked. The spin-coated sample in Fig. 1b) exhibited a mesoporous morphology with a crystal size of 30~40 nm, and countless TiO_2 nanoparticles formed the entire TiO_2 mesoporous layer. Meanwhile, the erosion of the Ti film due to the anodic oxidation current made the the anodized sample porous. Fig. 1a shows that the anodized film had a porous structure, and the diameter of the eroded holes was approximately 40 nm.
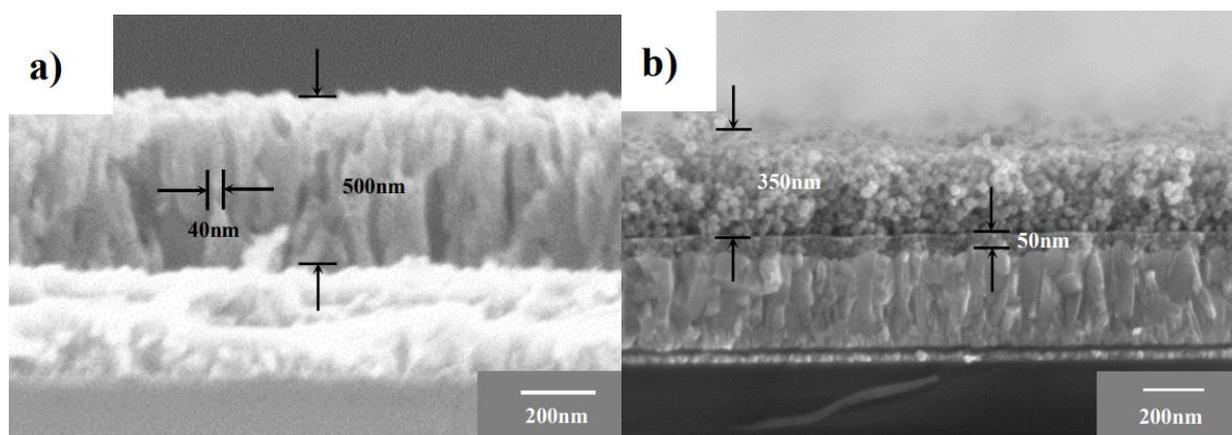
Figure 2. Cross-sectional SEM images of TiO_2 layers prepared by a) anodizing Ti/FTO substrate and annealing (Group A); b) spin-coating compact and mesoporous TiO_2 films and annealing (Group B).

Figure 2 shows the cross-sectional SEM images of TiO_2 ETLs to prepare PSCs in Group A and Group B. As shown in Fig. 2b), the ETL obtained by the spin-coating method consisted of two parts, where the TiO_2 dense layer and porous layer were approximately 50 nm and 350 nm thick, respectively. The anodized TiO_2 layer in Fig. 2a) exhibited an obvious tubular structure, where the TiO_2 nanotube layer was approximately 500 nm thick, and the tube wall was approximately 40 nm thick. Since the nanotubes were U-shaped structures, the thickness of the tube wall can be taken as the thickness of the dense layer, which was also 40 nm. As Fig. 2a) and Fig. 2b) show, because the dense layer and porous layer was separately spin-coated, the boundary between them was quite obvious, whereas the TiO_2 nanotubes obtained by anodization were integrated, and the bottom of the nanotubes acted as the dense layer. Fig. 2b) shows voids or cavities at the interface between the dense layer and the porous layer, which implies a more significant carrier loss at the interface and a shorter carrier lifetime.

In contrast, the anodization in Fig. 2a) did not show such problems.
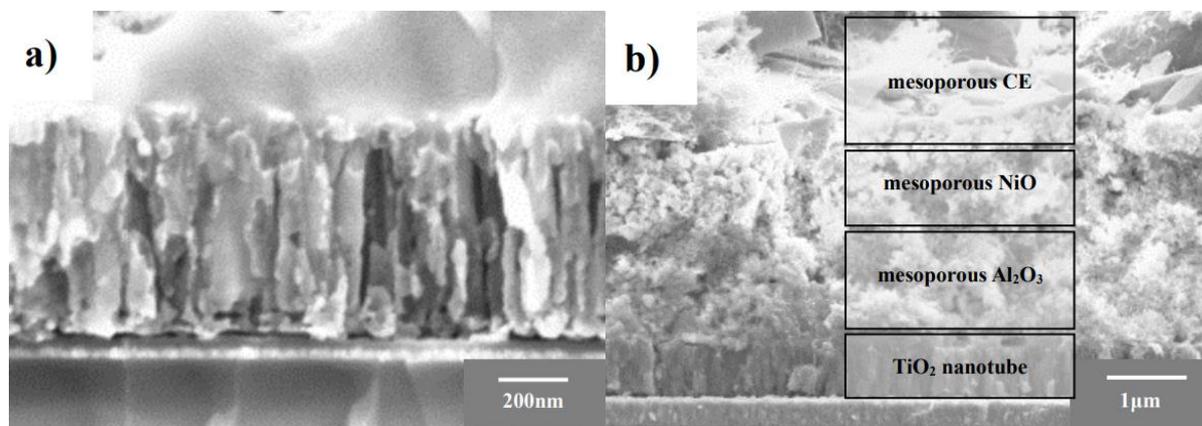
Figure 3. Cross-sectional SEM images of anodized PSCs in Group A: a) perovskite crystallized in TiO_2 nanotubes; b) anodized PSC consisting of TiO_2 nanotube/mesoporous Al_2O_3/mesoporous NiO/mesoporous CE.

Figure 3 shows the cross-sectional structure of the anodized samples. Figure 3a) clearly indicates that perovskite crystals were formed on the tube walls of anodized mesoporous TiO_2; thus, electrons generated by perovskite can be promptly transmitted to the TiO_2 nanotube wall. The structure of each layer in PSCs for Group A is shown in Fig. 3b). It is easily observed that the TiO_2 nanotube/mesoporous Al_2O_3/mesoporous NiO/mesoporous CE layers were sequentially deposited in FTO glass.

3.2 XRD analysis
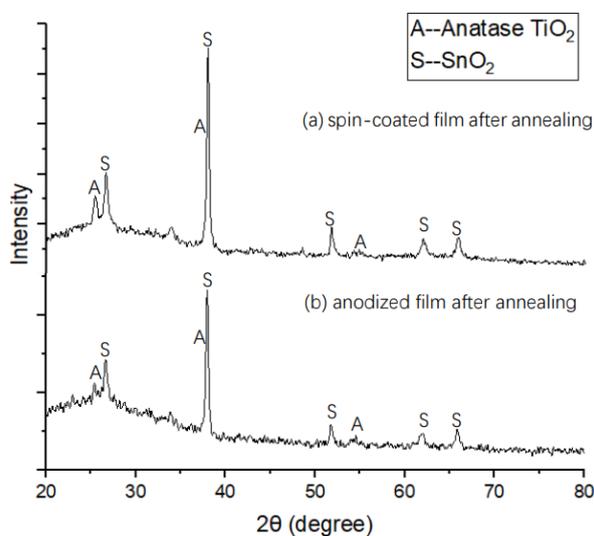
Figure 4. XRD patterns for TiO_2 films prepared by (a) anodizing Ti/FTO substrate and annealing; (b) spin-coating compact and mesoporous TiO_2 films and annealing.

Solid TiO_2 mainly has three crystalline phases: brookite, anatase, and rutile. Among them, anatase TiO_2 is ideal for PSCs due to its excellent electrical conductivity. To explore the crystallinity of ETLs made by anodization and spin-coating, XRD patterns of TiO_2 films were taken. The fabrication procedure of samples for XRD is introduced in Section 2.3. As shown in Fig. 4, the two samples had identical diffraction peaks, which shows that both methods can obtain anatase TiO_2. The difference between their intensities was due to the thickness difference between the two films.

3.3 Photovoltaic characteristics of PSCs

Table 1. Photovoltaic characteristics of PSCs in Group A (anodizing method) and Group B (spin-coating method)

	Sample	V_{OC} (V)	J_{SC} (mA/cm^2)	FF	PCE (%)
Group A	1-1	0.97	30.10	0.408	11.91
	1-2	0.92	31.54	0.442	12.83
	1-3	0.91	28.57	0.445	11.57
Group B	2-1	0.95	24.50	0.564	13.13
	2-2	0.93	25.23	0.546	12.82
	2-3	0.95	25.60	0.527	12.83

To explore the application of anodized TiO_2 ETLs in PSCs, the photovoltaic characteristics of both Group A and Group B were measured under AM 1.5G illumination, the fabrication procedure and characterization setup of which are elaborated in Section 2. The results are shown in Table 1.
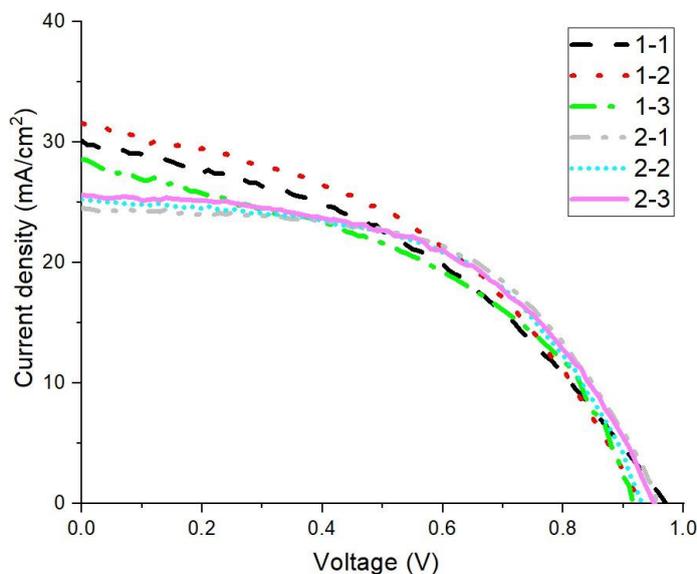
Figure 5. I-V curves of PSCs in Group A and Group B

According to the experimental results in Table 1, PSCs in Group A and Group B had similar distributions of V_{OC}, whose average was ~ 0.94 V. Meanwhile, the average PCEs of PSCs in Group A (12.10%) were slightly lower than those in Group B (12.93%). In contrast, J_{SC} was 30.07 mA/cm^2 on average in Group A and 25.11 mA/cm^2 in Group B.

V_{OC} is affected by the conduction band position of TiO_2 and electron lifetime in the conduction band [29]. The two groups of PSCs had similar conduction bands; thus, the difference in V_{OC} was mainly attributed to the difference in electron lifetime. For the samples in Group B, the voids or cavities at the interface between the dense layer and the porous layer may lead to carrier loss, which can shorten the lifetime of electrons, while the integral anodized ETLs had no such problems. Meanwhile, perovskite crystals in TiO_2 nanotubes were formed on the tube wall, and the contact area of perovskite crystals and TiO_2 nanotubes was smaller than that of perovskite crystals and spin-coated TiO_2 particles, which increased the carrier composite probability and shortened the lifetime of electrons for PSCs in Group A. Both samples in Group A and Group B had advantages in increasing the electron lifetime, so they had similar V_{OC} values.

J_{SC} is related to the surface contact area between TiO_2 layer and perovskite and the crystallinity of the TiO_2 layer [30], which corresponds to the charge separation, electron collection and transport. The crystallinity of ETLs in Group A and Group B had very few differences according to the XRD patterns in Section 3.2; thus, the main interference factor was the surface contact area with perovskite. The Samples in Group A had a thicker porous TiO_2 layer (500 nm) than those in Group B (350 nm); thus, more perovskite crystals were gathered in anodized ETLs, which resulted in a higher J_{SC}.

The efficiency of PSCs in Group A was relatively lower than that of samples in Group B, which was related to the fill factor (FF) of PSCs. The fill factor is related to the shunt resistance R_{sh} and series resistance R_s. For the samples in Group B, the contact area of perovskite crystals and spin-coated TiO_2 particles was wider; thus, the electrons transmitted in a wider channel. Therefore, the PSCs in Group B obtained a lower R_s, which implies a higher FF than the samples in Group B.

The present PCE of PSCs with anodized ETLs is significantly higher than that of solar cells with similar electron transport layers previously reported by Lei et al. [25] (8.07%) and Wang et al. [26] (8.31%), which are due to their low J_{SC} (14.36 mA/cm^2 and 15.46 mA/cm^2, respectively) [25, 26]. Furthermore, a perovskite solar cell without $TiCl_4$ treatment fabricated by Wang et al. [26] obtained a higher FF (0.63). This may be related to the narrower nanotube gap of TiO_2 ETL, which leads to a wider contact area of perovskite crystals and a higher FF.

Above all, the anodized samples in Group A had similar V_{OCS}, higher J_{SCS}, lower FFs and consequently lower PCEs than the spin-coated samples in Group B. Moreover, the anodized samples obtained a higher PCE than PSCs with similar electron transport layers.

4. CONCLUSION

A novel TiO_2 electron transport layer was synthetized by anodizing a Ti/FTO film in an ethylene glycol electrolyte with NH_4F and H_2O. The TiO_2 nanotube layer (porous layer) and compact layer were 500 nm and 40 nm, respectively, and the diameter of eroded holes in the porous layer was approximately 40 nm. After anodization and sintering, anatase TiO_2 was obtained. PSCs with anodized ETLs and spin-coating ETLs were fabricated and compared. PSCs with anodized TiO_2 ETLs had a maximum PCE of 12.82%, which was close to PSCs with spin-coating ETLs (13.13%).

Compared to the conventional spin-coating method, anodizing Ti/FTO can conveniently obtain integrated TiO_2 nanotubes and TiO_2 compact layers with fewer steps and defects. PSCs using anodized ETLs showed comparable efficiency with PSCs using spin-coating ETLs. Thus, the anodizing process will be a convenient and effective alternative to obtain TiO_2 ETLs for perovskite solar cells.

References

1. A. Kojima, K. Teshima, Y. Shirai, and T. Miyasaka, *J. Am. Chem. Soc.,*131 (2009) 6050.
2. M. M. Lee, J. Teuscher, T. Miyasaka, T. N. Murakami, and H. J. Snaith, *Science*, 338 (2012) 643.
3. H Min, D. Y. Lee, J. Kim, G. Kim, K. S. Lee, J. Kim, M. J. Paik, Y. K. Kim, K. S. Kim, M. G. Kim, T. J. Shin, and S. Seok, *Nature*, 598 (2021) 444.

4. K. Yoshikawa, H. Kawasaki, W. Yoshida, T. Irie, K. Konishi, K. Nakano, T. Uto, D. Adachi, M. Kanematsu, H. Uzu, and K. Yamamoto, *Nat. Energy*, 2 (2017) 17032.

5. K. Wojciechowski, T. Leijtens, S. Siprova, C. Schlueter, M. T. Hörantner, J. T. Wang, C. Li, A. K. Jen, T. Lee, and H. J. Snaith, *J. Phys. Chem. Lett.*, 6 (2015) 2399

6. J. T. Wang, J. M. Ball, E. M. Barea, A. Abate, J. A. Alexander-Webber, J. Huang, M. Saliba, I. Mora-Sero, J. Bisquert, H. J. Snaith, and R. J. Nicholas, *Nano Lett.*, 2014, 14 (2014) 724.

7. C. Kuang, G. Tang, T. Jiu, H. Yang, H. Liu, B. Li, W. Luo, X. Li, W. Zhang, F. Lu, J. Fang, and Y. Li, *Nano Lett*, 15 (2015) 2756.

8. W. Qiu, M. Buffiere, G. Brammertz, U. W. Paetzold, L. Froyen, P. Heremans, and D. Cheyns, *Org. Electron.*, 26 (2015) 30.

9. B. Conings, L. Baeten, T. Jacobs, R. Dera, J. D'Haen, J. Manca and H.-G. Boyen. *APL Mater.*, 2 (2014) 2423.

10. D. Liu and T. L. Kelly, *Nat. Photonics*, 8 (2014) 133.

11. Q. Jiang, L. Zhang, H. Wang, X. Yang, J. Meng, H. Liu, Z. Yin, J. Wu, X. Zhang, and J. You, *Nat. Energy*, 2 (2016) 16177.

12. D. Li, Y. Chen, P. Du, Z. Zhao, H. Zhao, Y. Ma, and Z. Sun, *RSC Adv.*, 5 (2015) 88973.

13. A. Kojima, K. Teshima, Y. Shirai, and T. Miyasaka, *J. Am. Chem. Soc.*, 131 (2009) 6050.

14. Y. Rong, Y. Ming, W. Ji, D. Li, A. Mei, Y. Hu, and Hongwei Han, *J. Phys. Chem. Lett.*, 9 (2018) 2707.

15. T. Bu, J. Li, F. Zheng, W. Chen, X. Wen, Z. Ku, Y. Peng, J. Zhong, Y. B. Cheng, and F. Huang, *Nat. Commun.*, 9 (2018) 4609.

16. Q. Jiang, X. Zhang, and J. You, *Small*, 14 (2018) 1801154.

17. I. S. Kim, R. T. Haasch, D. H. Cao, O. K. Farha, J. T. Hupp, M. G. Kanatzidis, and A. B. F. Martinson, *ACS Appl. Mater. Interfaces*, 8 (2016) 24310.

18. D. Xu, H. Hu, B. Lin, J. Ding, and N. Yuan, *Chem. Commun.*, 50 (2014) 14405.

19. M. H. Kumar, N. Yantara, S. Dharani, M. Graetzel, S. Mhaisalkar, P. P. Boix, N. Mathews, *Chem. Commun.*, 49 (2013) 11089.

20. E. H. Anaraki, A. Kermanpur, L. Steier, K. Domanski, T. Matsui, W. Tress, M. Saliba, A. Abate, M. Grätzel, A. Hagfeldt, and J. Correa-Baena, *Energy Environ. Sci.*, 9 (2016) 3128.

21. D. Zheng, G. Wang, W. Huang, B. Wang, W. Ke, J. L. Logsdon, H. Wang, Z. Wang, W. Zhu, J. Yu, M. R. Wasielewski, M. G. Kanatzidis, T. J. Marks, and A. Facchetti, *Adv. Funct. Mater.*, 29 (2019) 1900265.

22. T. S. Su, T. Y. Hsieh, C. Y. Hong, T. C. Wei, *Sci. Rep.*, 5 (2015) 16098.

23. V. Zwilling, E. D. Ceretti, A. B. Forveille, D. David, M. Y. Perrin, and M. Aucouturier, *Sur. Interface Anal.*, 27 (1999) 629.

24. S. P. Albu, A. Ghicov, J. M. Macak, and P. Schmuki, *Phy. Ptat. Sol. (RRL)*, 1 (2007) R65.

25. B. X. Lei, J. Y. Liao, Z. Ran, J. Wang, D. B. Kuang, *J. Phys. Chem. C*, 114 (2010) 15228.

26. X. Wang, Z. Li, W. Xu, S. A. Kulkarni, S. K. Batabyal, S. Zhang, A. Cao, L. H. Wong, *Nano Energy*, 11 (2015) 728.

27. J. Krysa, K. Lee, S. Pausova, S. Kment, Z. Hubicka, R. Ctvrtlik, and P. Schmuki, *Chem. Eng. J.*, 308 (2017) 745.

28. V. Ostapchenko, Q. Huang, Q. Zhang, and C. Zhao, *Int. J. Electrochem. Sci.*, 12 (2017) 2262.

29. Z. Yu, N. Vlachopoulos, A. Hagfeldt, and L. Kloo, *RSC Adv.*, 3 (2013) 1896.

30. J. Yang, Z. Gao, T. Li, P. Ma, D. Wu, and Y. Lin, *Micro Nano Lett.*, 6 (2011) 737.